HHS Public Access

Author manuscript

Macromol Biosci. Author manuscript; available in PMC 2021 December 01.

Published in final edited form as:

Macromol Biosci. 2020 December ; 20(12): e2000183. doi:10.1002/mabi.202000183.

Rheological Properties of Coordinated Physical Gelation and Chemical Crosslinking in Gelatin Methacryloyl (GelMA) Hydrogels

Ashlyn T. Young[1], **Olivia C. White**[2], **Michael A. Daniele**[1,2,*]

[1]Joint Department of Biomedical Engineering, North Carolina State University and University of North Carolina, Chapel Hill, 911 Oval Dr., Raleigh NC, 27695 (USA)

[2]Department of Electrical & Computer Engineering, North Carolina State University, 890 Oval Dr., Raleigh NC, 27695 (USA)

Abstract

Synthetically-modified proteins, such as gelatin methacryloyl (GelMA), a.k.a. gelatin methacrylate or gelatin methacrylamide, are growing in popularity for bioprinting and biofabrication. GelMA is a photocurable macromer that can rapidly form hydrogels, while also presenting bioactive peptide sequences for cellular adhesion and proliferation. The mechanical properties of GelMA are highly tunable by modifying the degree of substitution via synthesis conditions, though the effects of source material and thermal gelation effects have not been comprehensively characterized at lower concentration gels. Herein, we investigate the effects of animal source and processing sequence on scaffold mechanical properties. Hydrogels of 4-6 wt% were characterized. Depending on the temperature at crosslinking, the storage moduli for GelMA derived from pigs, cows, and cold-water fish range from 723-7340 Pa, 516-3484 Pa, and 294-464 Pa, respectively. The maximum storage moduli are achieved only by coordinated physical gelation and chemical crosslinking. In this method, the classic physical, thermo-reversible gelation of gelatin occurs when GelMA is cooled below a thermal transition temperature, which is subsequently 'locked in' by chemical crosslinking *via* photocuring. The effects of coordinated physical gelation and chemical crosslinking are demonstrated by precise photopatterning of cell-laden microstructures, inducing different cellular behavior depending on the selected mechanical properties of GelMA.

TABLE OF CONTENTS

We investigate the effects of animal source and processing sequence on the rheological properties of gelatin methacryloyl gels. The effects of coordinated physical gelation and chemical crosslinking are demonstrated by precise photopatterning of cell-laden microstructures, inducing different cellular behavior depending on the selected mechanical properties of the GelMA.

Graphical Abstract

[*]Correspondence: mdaniel6@ncsu.edu.

ELECTRONIC SUPPLEMENTATRY INFORMATION

Electronic Supplementary Information is available free of charge online at https://pubs.acs.org., including rheometry frequency sweeps, curing point measurements, temperature sweeps, image processing schematic, and spheroid proliferation analyses.

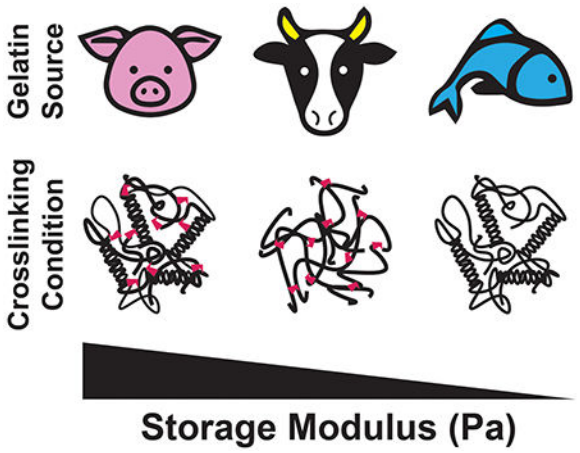

Keywords

GelMA; photopolymerization; mechanical properties; gelatin methacryloyl; gelation; animal source; gelatin

INTRODUCTION

The native extracellular-matrix (ECM) is comprised of many macromolecules, providing a tissue-specific environment for cellular interaction, function, differentiation, and proliferation.[1] The most abundant protein present in ECM is collagen, characterized by triple-helix fibrils with diameters ranging from approximately 12 to 500 nm.[2–3] These fibrils provide key structural support in the ECM, and possess bioactive peptide sequences for cell adhesion and proliferation.[4–5] Furthermore, collagen plays a role in cell differentiation and regulation, suggesting the integration of collagen into bio/synthetic matrices may be critical to achieve physiologically accurate tissue function.[6–7] Specifically, tuning collagen concentration and matrix stiffness has been shown to affect lineage specification and activation of mesenchymal stem cells due in part to resultant cell morphology, focal-adhesion structure, and the binding of integrin adhesion receptors to available ECM components.[8–10] Unfortunately, collagen is neither easily chemically-modified nor processible. Modification of collagen is primarily limited by availability of accessible functional groups, *e.g. free* amines, thus requiring more complex modification strategies to generate the desired macromers.[11–14] Collagen exhibits thermal gelation reversibility, limited mechanical strength, batch-to-batch variability, and high cost. To address these disadvantages, collagen triple helices can be denatured or chemically-modified. Gelatin—the product of hydrolyzing collagen—is a single strand biopolymer containing lysine groups, presenting free amines, that can be modified to create a processible biopolymer.[15] Gelatin methacryloyl (GelMA), *a.k.a.* gelatin methacrylate or gelatin methacrylamide, is a methacrylate-functionalized gelatin that can undergo free radical polymerization.[16–18]. The mechanical properties of GelMA are tunable by changing the crosslink density *via* controlling the degree of substitution (DS) during synthesis, changing the weight percent solids in the desired hydrogel, amount of photoinitiator, and processing conditions, such as temperature or irradiation power. Basic mechanical properties of thermally gelled and

photocured GelMA have been characterized and typical GelMA moduli lie within a suitable range for tissue engineering (<100 Pa to 30 kPa).[16, 19–21]

Gelatin obtained *via* hydrolysis of collagen sourced from different animals are known to have different physical and chemical properties.[22–24] The most widely used gelatins for GelMA synthesis is derived from bovine and porcine collagen, though cold-water fish derived gelatin has been explored for temperature sensitive applications due to its much lower melting point.[25–27] Gelatin is hydrolyzed from collagen through acidic, alkaline, or enzymatic methods. Type-A gelatin is obtained through acidic hydrolyzation of collagen, and type-B gelatin originates from alkaline hydrolysis.[22] Treatment processes can affect final properties of gelatin and GelMA, resulting in a range of physico-chemical properties and available functional groups for modification.[28–29] Type A gelatin has been reported to have more free carboxyl groups and a higher isoelectric point compared to type B. Porcine skin gelatin is most commonly type A and bovine skin gelatin is most often type B. Gelatin from different animal sources is also reported to have different amino acid contents, molecular weights, and isoelectric points.[25, 28] These characteristics have been analyzed in unmodified gelatin, comparing porcine, bovine, and piscine originated materials.[28, 30] Mammalian gelatin is well characterized, exhibiting Bloom strengths, higher imino acid content, and higher molecular weights when compared to cold-water fish gelatin.[30] Furthermore, when comparing mammalian gelatin from porcine and bovine sources, porcine gelatin has higher glycine and proline content, as well as higher gel strength.[28] Most gelatin characterization is motivated by applications in the food science field as an additive, stabilizer, or clarifying agent.[15, 31] Studies directed toward modified gelatin for tissue engineering applications are distributed across many reports, though information on unmodified gelatin remains valuable as many unmodified gelatin properties are conserved in GelMA.

Processing and operational temperature also play important roles in the mechanical properties of GelMA hydrogels. GelMA, like gelatin, undergoes physical gelation at a sol-gel transition temperature. When gelatin is cooled below the gel point, it undergoes a conformational transition from a coiled polymer to a helical collagen-like structure.[32–34] Weak hydrogel bonds form between gelatin and water, creating a disorganized nest of partial helices and trapped water. This gel will revert to solution once heated above the transition temperature. Although gelatin hydrogels have mechanical properties that would be appropriate for a 3D tissue engineering, applications are limited due to the material returning to liquid form at human core body temperatures (37°C).

By comparison, GelMA hydrogels can maintain favorable physical properties across a wider temperature range, due to the presence of irreversible covalent crosslinks. As GelMA hydrogel properties are highly process dependent, reports of the mechanical properties are poorly consolidated and vary due to processing variables such as gelatin source, synthesis methods, concentration, polymerization temperatures, etc.[16–18, 20, 23, 35–38] GelMA undergoing physical gelation followed by chemical crosslinking has been described previously by Rizwan *et al.* as a method to fabricate stiff, patterned substrates for use in corneal tissue engineering.[39] This group briefly reported mechanical properties of physical and chemically crosslinked ‘GelMA+’ synthesized from type A gelatin with unreported

Bloom strength. They used compressive testing to confirm an 8-fold increase in mechanical strength as compared to chemical crosslinking alone, testing GelMA concentrations of 10 wt % and higher with 0.5 wt% Irgacure 2959 photoinitiator. Zaupa *et al.* also reported an increase in compressive modulus upon physical and chemical crosslinking, including a 15-fold increase for bovine-derived GelMA with a 220 g Bloom strength at a 10 wt% concentration with 0.2 wt% Irgacure 2959 photoinitiator.[7] Compressive modulus of materials physically and chemically crosslinked were also assessed at a 40 wt% concentration with 0.5 wt% Irgacure for applications in creating microspheres for cell experiments.[40] Most recently Park *et al.* demonstrated the temperature effects on the mechanical properties of GelMA, specifically analyzing type A porcine-derived GelMA with a 300 g Bloom strength and a 60% DS.[41] All reported measurements by Park *et al.* were made at a 35 wt% concentration hydrogels, which exceeds commonly demonstrated ranges for 3D cell cultures and bioprinting. Many prior reports investigate dual crosslinking at high concentrations (>10 wt%), which is not particularly useful for embedded cell proliferation and organization *in vitro*. Low concentration GelMA, around 5%, with lower DS has been reported to better support embedded cell proliferation, sprouting, and network formation, particularly for vasculature cells. [17, 21] Accordingly, we seek to expand on that report by investigating a range of GelMA concentrations and sources more suitable to 3D cell culture and bioprinting. Other methods for enhancing mechanical properties of GelMA have been reported, primarily by adding additional materials for reinforcement. Examples include PEG-derivatives, bioglass, graphene oxide, alginate, and even unmodified gelatin. [36, 42–47]

Herein, we take advantage of the unique properties enabled by physical gelation by coordinating thermal and chemical crosslinking to achieve both physically and covalently crosslinked GelMA hydrogels. GelMA is thermally annealed at 4°C to induce substantial thermal gelation, and subsequently photocured to create chemical crosslinks. When GelMA is chemically photopolymerized while in the gelled state, otherwise temporary complex structures and hydrogel bonds are ‘locked in’ by chemical crosslinks. Therefore, a stiffer hydrogel is formed, with physical and chemical crosslinks conserved at body temperature. This phenomenon may explain variations in reported GelMA mechanical properties, as consistent temperature conditions are not always reported in published studies. Furthermore, we utilize coordinated physical gelation and chemical crosslinking and chemical crosslinking alone to pattern scaffolds, resulting in proximal scaffolds with variable mechanical properties created with the same precursor material. We characterize the rheological properties of GelMA hydrogels with coordinated physical gelation and chemical crosslinking at low concentrations suitable for tissue engineering scaffolds. We demonstrate the ability to tune mechanical properties of GelMA in three ways: varying available methacryloyl groups to form covalent crosslinks, the selection of gelatin animal source, and processing temperatures. We also use thermal processing and photolithography to pattern GelMA and analyze the morphology of human dermal fibroblasts in response to varying scaffold stiffnesses. Lastly, we demonstrate the effect of thermal processing of GelMA on the proliferation of integrated cells by analyzing the sprouting and expansion of embedded tissue spheroids.

Through characterizing the mechanical properties of GelMA synthesized with different gelatin animal sources and degrees of substitution, as well as polymerized at different temperatures, we offer a consolidated report of the many metrics that must be taken into consideration when using GelMA for biomedical applications. Even further, we demonstrate the utility of tuning these metrics to elicit different cellular responses from both adherent and embedded cells.

RESULTS & DISCUSSION

The chemical and physical properties of unmodified gelatin from different animal sources has been reported, and a wide range of mechanical properties has been achieved.[28, 30–31, 38] Particular attention has been paid to the difference between cold-water fish and mammalian derived gelatins.[30–31] Not only are differences apparent in the rheological properties, but also in amino acid composition, Bloom strength, and isoelectric point. This information for the most common gelatin is provided in Table 1.

Bloom strength is a metric to define the strength of a gel, defined as the weight in grams required to depress a plunger into a gelatin sample by 4mm.[48] Gelatin must be cooled at 10°C for 16-18 hours prior to a Bloom test. Cold-water fish gelatin does not gel at 10°C, therefore Bloom strength is not reported. We observed each gelatin source varies in color, opacity, powder consistency, and solubility (*data not shown*). We have quantitatively demonstrated characteristics specific to origin and processing method for multiple GelMA types and degrees of substitution by colorimetric assays to quantify available primary amines and oscillatory rheology for mechanical property characterization. A key feature differentiating mammalian derived GelMA from cold-water fish derived GelMA is the ability to form reversible physical gels at temperatures above 10°C, which can be exploited to tune the physical properties of GelMA hydrogels. We demonstrate *'locking in'* of the physical networks typically only present below the sol-gel transition temperature, through successive chemical crosslinking *via* photocuring (Figure 1). The rheological and swelling properties of GelMA hydrogels that underwent coordinated physical gelation and chemical crosslinking were compared to those just photocured. The application of the coordinated crosslinking technique was demonstrated with human cells cultured on 2D patterned gels, as well as proliferation and migration from embedded tissue spheroids.

Degree of substitution.

We used a conventional trinitrobenzene sulfonic acid (TNBSA) assay to quantify free primary amines in unmodified and modified gelatin. For unmodified gelatin samples from different animal sources, porcine had the most available free amines and piscine had the least available free amines (Figure S2b). Available primary amines may be attributed to processing technique, Bloom strength, and molecular weights of unmodified gelatin. It has been previously reported that gelatin with different Bloom strength, from different suppliers, has differing lysine content, identifying a direct correlation between Bloom strength and lysine content.[49]

GelMA was synthesized with different amounts of methacrylic anhydride, referred to as 'Low' (93.75 μL MA, or 0.63 μM MA, per g Gelatin, 'Mid' (375 μL MA, or 2.5 μM MA,

per g Gelatin) and ‘High’ (750 μL MA, or 5.0 μM MA, per g Gelatin). DS was calculated from the ratio of free amines in modified gelatin and unmodified gelatin. DS increases for increasing amount of methacrylic anhydride, except for piscine GelMA, which showed similar DS for the medium and high amount of methacrylic anhydride, added (Figure S2a). The maximum DS for piscine GelMA was determined to be around 75%. Furthermore, considering porcine and bovine GelMA consisted of similar degrees of substitution for reaction condition and the available free amines were highest in porcine GelMA, porcine GelMA must consist of the most available groups to be covalently crosslinked at the same reaction conditions. This finding is consistent with rheological data collected. GelMA synthesis reaction parameters have been tuned via buffer pH adjustment to ensure reaction conditions are optimized depending on the isoelectric point of gelatin.[50] Considering isoelectric points for type A and type B gelatin vary, reaction conditions can be optimized depending on these values to increase DS. The range of DS is relatively small in this study, with the lowest DS higher than 25%, as compared to other studies, which report DS as low as 7%.[18, 51] Very low DS GelMA, at a low concentration, will not reach an extent of crosslinking necessary to form a solid gel to support cell culture or micropatterning; therefore, we restricted the DS to values in which a free-standing hydrogel could be formed.

Crosslinking kinetics of GelMA derived from different animal sources.

The crosslinking kinetics of GelMA from each animal source at Low, Mid, and High DS was measured using a parallel plate rheometer with UV curing accessories. The GelMA samples were photocured at 5 $mW{\cdot}cm^{-2}$ for 300 seconds. GelMA samples were tested at a concentration of 5 wt% with 0.5 wt% Irgacure 2959 photoinitiator. This concentration was chosen due to the favorable embedded cell properties at low weight percent GelMA, allowing cell outgrowth and sprouting depending on cell type.[17, 52–54] High weight percent hydrogels often result in limited cell migration and proliferation, longer degradation times, limited remodeling, and poor bio-integration. Before curing, samples were stored at 37 °C, as to be in a sol phase. Upon exposure to UV light, samples cured over time as demonstrated by the increasing storage modulus (G’) (Figure 2a–c). The cure points were calculated by taking the second derivative of the storage modulus (G’), defining where the rate of increase of the storage modulus (G’) begins to decrease (Figure S6b). The gel points were determined by identifying where the loss modulus (G’’) and storage modulus (G’) intersect ($\tan(\delta) = 1$) (Figure S6a). Although gel points are informative for defining the transition of GelMA from a liquid to a solid material, we consider curing points more appropriate for discussion in this study. Cure points are a more suitable metric for defining the UV exposure necessary to achieve a solid scaffold that is freestanding, defined the end of the curing process, and can support 3D cell culture. The higher the curing point, the longer it takes the material to polymerize, which is a critical parameter for 3D tissue engineering and bioprinting. We found that piscine GelMA had higher curing points at all degrees of substitution compared to porcine and bovine GelMA. We also found that for bovine GelMA, the curing point was highest for the lowest DS. The curing point is important to consider when utilizing biopolymers with living cell populations for tissue engineering. Most 3D bioprinters operate in a UV intensity between 0 and 30 $mW{\cdot}cm^{-2}$. Moreover, 3D bioprinters that additively generate structures, *i.e.* consist of many consecutive layers cured using a flood lamp, require fast curing materials to limit the radiation dose delivered to the resident cell populations. To

maintain bioprinting capability and cell viability with reasonable curing points, it is important to rapidly polymerize scaffolds at low light intensity. Using the same measurement technique, we calculated the curing point necessary for samples at increasing UV intensities. For all tested GelMA compositions, curing points are less than 30 seconds when cured at 30 $mW \cdot cm^{-2}$ (Figure 3). Low DS piscine gels took longer than 30 seconds to cure when exposed to UV light at less than 25 $mW \cdot cm^{-2}$. For all other GelMA compositions, curing points were longer than 30 seconds when UV light intensity was below 15 $mW \cdot cm^{-2}$.

Storage moduli of GelMA from different animal sources.

Storage moduli for GelMA synthesized from porcine, bovine, and cold-water fish gelatin sources were measured over a range of frequencies using a parallel plate rheometer. After curing using a UV rheometer accessory, a frequency sweep was performed from 0.1 Hz to 10 Hz at 1% strain at room temperature. All GelMA samples demonstrated consistent storage modulus (G') measurements across the entire frequency sweep (Figure S3). Storage modulus (G') values were averaged across frequencies and compared to determine changes in mechanical properties across GelMA samples from different animal sources and degrees of substitution (Figure 4a–c). Rheological analysis was also performed at 37°C, with results collected at room temperature versus cell culture temperature in similar ranges, confirming conclusions drawn from rheological characterization at room temperature can be applied to cellular assays performed at 37°C (Figure S13). Storage modulus (G') data agreed with TNBSA measurements, demonstrating that more available crosslink groups results in gels with a higher storage modulus (G'). Generally, storage moduli (G') are lower for GelMA synthesized from gelatin with lower molecular weights and available crosslink groups. For all degrees of substitution, porcine GelMA had the highest storage moduli compared to other animal source. High and mid degrees of substitution did not have significant changes in storage modulus (G') for porcine GelMA, and both were significantly higher than porcine GelMA with the lowest DS. Bovine GelMA did not have significantly different storage moduli with different degrees of substitution, suggesting available methacrylate groups affects time to gel but not final mechanical properties for GelMA. Piscine GelMA had the lowest storage moduli for all degrees of substitution, with non-significant differences in storage moduli for high and mid degrees of substitution, and the lowest storage modulus (G') of all the samples for the low DS gels. Consequently, crosslinking kinetics and final material properties are different for GelMA from different animal sources and with different degrees of substitution.

Coordinated physical gelation and chemical crosslinking in GelMA.

Free-radical photopolymerization of GelMA results in chemical crosslinks between methacrylamide and methacrylate groups on the gelatin backbone.[55–56] This randomly organized crosslinking strategy results in hydrogels that have proportionally stronger mechanical properties with higher available crosslinks, controlled by the DS during synthesis or the available free amines for modification in gelatin.[18] Storage modulus (G') is highest for GelMA hydrogels with the highest DS. When crosslinked above the sol-gel transition temperature, these covalent crosslinks are the determining factor for final mechanical properties. When below the sol-gel transition temperature, gelatin undergoes

physical gelation, where the gelatin backbone attempts to reorient into a partially coiled collagen-like structure. This is characterized by a mixture of coil-like structures, as well as random weak hydrogen bonds between gelatin backbones. This gel will revert to liquid upon heating above the transition temperature in gelatin. Interestingly, GelMA demonstrates physical gelation, much as unmodified gelatin, and available methacryloyl groups can facilitate chemical crosslinking after physical gelation. This results in a final gel that maintains physical bonds due to backbone proximity being conserved by chemical crosslinks. With rheological frequency sweeps collected as described previously, it is demonstrated that GelMA photocured after incubation at 4°C degrees (after physical gelation) has up to an 8x higher storage modulus (G') compared to chemical crosslinking alone (Figure 4a–c). Porcine GelMA hydrogels remain stronger than bovine GelMA hydrogels, consistent with rheological data of chemical crosslinking alone, which is as expected considering porcine gelatin has both a larger Bloom strength and more available groups for chemical crosslinking. Piscine GelMA hydrogel's mechanical properties are the same regardless of polymerization after incubation at 37°C or 4°C because physical gelation does not occur. Differences in mechanical strength due to DS is conserved when polymerized after physical gelation. Porcine GelMA trends were consistent, with GelMA consisting of higher degrees of substitution possessing a higher mechanical strength under coordinated crosslinking. Bovine GelMA with coordinated crosslinking also demonstrates mechanical properties that are not significantly different for samples with different degrees of substitution.

Initial storage moduli for porcine and bovine GelMA is between 100 and 1000 Pa due to physical gelation of the sample prior to testing (Figure 4d–f). Although increased DS results in stronger gels after chemical crosslinking, samples that are only physically gelled exhibit the inverse response. GelMA with higher degrees of substitution result in softer gels when only undergoing physical gelation. This may be due to methacryloyl groups impeding random physical bonds, causing a weaker network in GelMA with higher degrees of substitution.

Swelling properties of GelMA.

Crosslink density and molecular weight between crosslinks is directly correlated to water content in a hydrogel, affecting the diffusion of nutrients and the mesh size, which influences cell migration and adhesion.[57–58] Swelling properties were used to determine the molecular weight between crosslinks ($\overline{M_c}$) for GelMA from different animal sources and with different degrees of substitution (Figure S7). Swelling ratio (Q) was calculated using the weight of the swollen gel (W_s) and the weight of the dry gel (W_d) with Equation 1:

$$Q = \frac{W_s}{W_d} \quad (1)$$

GelMA polymerized at 37 °C demonstrated higher swelling ratios then those calculated for GelMA polymerized at 4 °C, except for piscine GelMA, which remained the same (Figure S7). The $\overline{M_c}$ was calculated using Equation 2 derived from the Theory of Rubber Elasticity:

$$\overline{M_c} = \frac{1}{\left(\frac{G}{cRTQ^{-1/3}}\right) + \left(\frac{2}{M_n}\right)} \quad (2)$$

Using the measured shear modulus (G) and swelling ratio (Q), the defined concentration (c) and molecular weight (M_n) of GelMA, as well as the universal gas constant (R) and absolute temperature (T), we can determine $\overline{M_c}$ for each GelMA sample processed at different crosslinking conditions. Molecular weight values were determined based on ranges determined from Bloom strength provided from the supplier (Table 1). While the Theory of Rubber Elasticity may not fully describe the crosslinking and gelation mechanism of the described system, it has been used previously to describe $\overline{M_c}$ in thermally-gelled gelatin[59–61] and to quantify the $\overline{M_c}$ in covalently-crosslinked GelMA and other covalently-crosslinked hydrogels.[62–65] Further exploration of the synergistic or interfering effects of concurrent covalent and physical crosslinking may offer valuable insight into the fundamental development of GelMA hydrogels and may be explored in future efforts. Herein, we report the calculated $\overline{M_c}$ from both rheological and swelling characterization for GelMA hydrogels derived from different animal sources and processed at different temperatures. The molecular weight between crosslinks were higher for GelMA polymerized after incubation at 37 °C compared to GelMA polymerized after incubation at 4°C (Table 2). The difference in molecular weight between crosslinks between the same GelMA materials crosslinked at different temperature is described as $\Delta\overline{M_c}$, with the percent increase of $\overline{M_c}$ for GelMA polymerized at 37° compared to $\overline{M_c}$ for GelMA polymerized at 4°C shown in parentheses. Photocuring porcine gelatin, after incubation at 37°C, resulted in a greater than 200% increase in $\overline{M_c}$. For the same conditions, bovine GelMA exhibited an 86% increase. Piscine values were similar with only a 10% change calculated between processing temperatures. These calculations confirm that porcine and bovine GelMA with coordinated physical and chemical crosslinking have shorter molecular weight between crosslinks, increased crosslink density, and reduced mesh size, resulting in less swelling. This dense network contributes to much higher storage moduli when compared to samples chemically crosslinked alone, suggesting that GelMA that undergoes consecutive physical gelation and chemical crosslinking increases crosslink density.

Effect of processing temperature during chemical crosslinking of GelMA.

The rheological properties of porcine GelMA photocured after incubation at 37°C and 4°C was characterized under a temperature sweep from 4°C to 50°C to investigate the effect of processing temperature on the subsequent properties of the GelMA hydrogels. Specifically, we aimed to investigate if any reversible physical gelation of GelMA was still exhibited after photocuring (Figure 5). Photocuring after incubation at 4°C increased the storage modulus (G') compared to photocuring after incubation at 37°C. For comparison, we calculated the percent change in the storage modulus (G') between the peak temperature (50°C) and minimum temperature (4°C). GelMA hydrogels created from materials with low DS exhibited the greatest difference in storage modulus (G') across the temperature sweep. For Low GelMA hydrogels photocured after incubation at 4°C and 37°C, the change in storage

modulus (G') was 21% and 81%, respectively. A similar trend was exhibited for both the Mid and High GelMA hydrogels. This effect is attributed to the conserved ability for the GelMA hydrogels to undergo reversible physical gelation. Specifically, in GelMA hydrogels that have coordinated physical gelation and chemical crosslinking, *i.e.* photocured after incubation at 4°C, the initial physical gelation "pre-organizes" the GelMA and a lesser variation in storage modulus (G') is exhibited.

Furthermore, increasing the DS reduces the storage modulus (G') difference across the temperature sweep for GelMA hydrogels that have coordinated physical gelation and chemical crosslinking. This may be attributed to the higher degree of substitution, *i.e.* increased crosslink density, acting as an irreversible means to "lock in" the physically gelled state; therefore, lesser re-organization occurs during the temperature sweep. Interestingly, High DS GelMA polymerized after incubation at 4°C shows a change in storage modulus (G') of 49%. This can be attributed to fewer bonds due to physical gelation as compared to Low and Mid DS. As discussed previously, when only physically gelled at 4°C, GelMA with the High DS has a lower storage modulus (G') when compared to Low and Mid DS, due to methacryloyl groups impeding the formation of physical bonds upon gelation. Therefore, for GelMA with coordinated physical gelation and chemical crosslinking, chemical crosslinks are in a much higher abundance than physical bonds. This phenomenon may explain the higher change in storage modulus across a temperature sweep when compared to the change in storage modulus for GelMA with a lower DS. In contrast, in GelMA hydrogels that do not have coordinated physical gelation and chemical crosslinking, *i.e.* photocured after incubation at 37°C, there is an inverse relationship between DS and change in storage modulus (G') across the temperature sweep. This supports the reasoning that the lower crosslink density for low DS hydrogels increases the degrees of freedom for the GelMA to form a physical gel. Overall, GelMA with coordinated gelation and crosslinking shows a lesser change in storage moduli over the temperature sweep when compared to GelMA with chemical crosslinking alone.

Human dermal fibroblast morphology on porcine GelMA.

Scaffold mechanical properties play a key role in cellular proliferation, differentiation, adhesion, and migration. Tissues have different storage moduli, ranging from 0.5 to 20000 kPa for fat and bone, respectively.[66–67] One way to characterize cellular response to substrate stiffness is through determining morphological patterns and cytoskeletal organization. We observed human dermal fibroblast (HDFn) response to GelMA stiffness, modulated by temperature at crosslinking. HDFn actin structure distribution and proliferation rates have been shown to vary depending on scaffold properties.[68–70] HDFns were seeded on polymerized porcine GelMA scaffolds and morphological properties were quantified to demonstrate a cellular response to substrate stiffness. High DS porcine GelMA at a low concentration of 4 wt% were used for this analysis. We selected 4 wt% GelMA because concentrations of 5 wt% or less, while difficult to bioprint due to low viscosity, demonstrate improved cellular viability, sustained proliferation, and exhibit modulus ranging from 0.25-1.5 kPa.[71–75] In our experiments, scaffolds polymerized at 4°C possessed coordinated physical gelation and chemical crosslinking, resulting in a stiffer scaffold.

HDFns seeded on coordinated gelation and crosslinked scaffold demonstrated an elongated morphology (Figure 6a).

Alternatively, HDFns seeded on GelMA scaffolds polymerized above the gel point at 50°C, demonstrated a round morphology (Figure 6b). The morphology of the cells cultured on different scaffold stiffnesses were quantified by determining the aspect ratio, where an aspect ratio of 1 described a circular cell. Cells growing on the softer surface, polymerized at 50°C, had a significantly lower aspect ratio compared to cells grown on stiffer scaffold that was polymerized at 4°C (Figure 6c).

Spatial organization of cells was also demonstrated through patterning scaffold polymerization at different temperatures using a photomask. A porcine GelMA scaffold was cooled to 4°C and polymerized under a striped photomask, heated to 50 °C, and repolymerized without a photomask. This resulted in lines of softer GelMA alongside stiffer GelMA (Figure 7d). The cellular morphologies observed on stiff or soft scaffolds (Figure 7a–b) can be seen along patterned lines corresponding to crosslinking conditions during photomasking (Figure 7c). Through these results, we can conclude that photomasking with coordinated gelation and crosslinking is a suitable method for patterning stiff substrates alongside much softer substrates without requiring multiple materials. Microfabrication of unique structures with variable stiffnesses has utility in the fabrication of biomimetic cell culture scaffolds, specifically for co-culture models and controlling stem cell fate via material stiffness.[76–77] Typically, scaffold patterning with variable stiffness requires multiple precursor materials and fabrication steps, limiting resolution and feasibility. Pairing traditional GelMA photo-crosslinking with coordinated gelation and crosslinking provides a new tool for spatially patterning hydrogel scaffolds for tissue engineering applications in 2D and 3D.

MDAMB231 Spheroid Outgrowth in GelMA.

Cells respond to environmental conditions much differently when adherent in 2D compared to embedded in 3D.[78] Adherent cells grown on 2D surfaces tend to polarize and spread depending on substrate properties, and form planar protein adhesions to the culture surface. Alternatively, in 3D cultures cells have no prescribed polarity and can spread in any direction depending on available adhesion proteins and chemical gradients. Due to the highly dynamic nature of 3D culture, and tendency for cells to migrate and spread, scaffold considerations are much different in 3D compared to 2D cultures. Cells embedded within scaffolds are limited in size, shape, and proliferation capabilities depending on the matrix material properties, crosslinks, bioactive groups, and water content. Without the conditions necessary for cell invasion and proliferation into a scaffold, cells will remain spherical and will not interact with the surrounding matrix to provide a dynamic tissue structure despite maintaining high viability.[17] Cellular response to surrounding matrices are of importance when designing scaffold structures for tissue engineering or bio-integration applications. Despite GelMA possessing RGD groups, which allow cells to integrate and adhere to the scaffold, without the appropriate porosity, water content, and mechanical properties, dynamic integration of cellular networks will not be achieved. Even further, optimal environments for cell proliferation varies depending on cell type and desired application.

Some cells prefer softer matrices, while others display peak activity in matrices with stiffer and denser fibers.[79–80] The tunable nature of GelMA depending on material source, DS, concentration, and processing temperatures suggests broad applications in tissue engineering, as long as both the sourcing and processing parameters are defined to achieve the desired material properties.

To demonstrate embedded cell activity dependence on scaffold properties, we embedded MDAMB231 spheroids inside of porcine and cold-water fish GelMA with different degrees of substitution and temperature at crosslinking. MDAMB231 cells are human epithelial mammary adenocarcinoma cells that will invade surrounding matrices when cultured into spheroids. MDAMB231 spheroids formed, after culturing in a cell repellent round-bottom plate in complete medium supplemented with 3.5 wt% Matrigel for 3 days. After culturing, spheroids were embedded in low, mid, and high DS porcine or piscine GelMA. GelMA with embedded spheroids were incubated at 37°C or 4°C for 10 minutes prior to UV exposure at 10 $mW \cdot cm^{-2}$, and culture medium was added on top of polymerized gels. Brightfield images were collected after polymerization and quantified by measuring the integrated radial profile around the spheroid edge. Using radial profile measurements, we compared GelMA scaffold effects on spheroid core size, measuring cell aggregates in the center of the spheroid without measuring the cells sprouting outward or detached. The radius of the spheroid core is identified as maximum intensity radius from integrated radial profile measurements (Figure S10). Prior to embedding in GelMA, spheroids were 272 ± 72 μm in diameter. All spheroids reduced in size upon embedding into a GelMA scaffold compared to sizes prior to embedding. Spheroid size immediately after embedding in GelMA varied depending on GelMA properties, with stiffer gels generally resulting in larger spheroids (Figure S12a). The largest resultant spheroids were those embedded in porcine GelMA polymerized at 4°C. For spheroids embedded in porcine GelMA and photocured at 37°C, an inverse relationship was observed between DS and spheroid diameter. While it has been demonstrated that increasing GelMA stiffness results in smaller spheroids, this property is typically controlled by total concentration of GelMA. We hypothesize that the observed effect of DS and temperature on initial spheroid size may be attributed to the different gelling kinetics between Low and High DS GelMA. After four days of culture, spheroids were fixed, stained, and imaged to determine core size and outgrowth. Spheroid viability was confirmed using live/dead stain (Figure S11). As expected, spheroid core decreased in size after culture for stiffer gels, such as porcine GelMA photocured at 4°C. (Figure S12b). It is known that compressive stresses will prevent spheroid growth due to volume constraints, an effect observed with various spheroid and scaffold types.[81–84] We observed the most limited growth in porcine GelMA polymerized at 4°C, where we also observed the scaffold radially shrinking over time. Acellular porcine GelMA with high DS polymerized at 4°C in a well plate exhibited a 28.7 ± 2.1% decrease in scaffold diameter 3 days after crosslinking. When polymerized at 37°C there was a 12.7 ± 0.54% decrease in scaffold diameter 3 days after crosslinking, significantly less collapse than samples polymerized at 4 °C. The exhibited scaffold collapse, when polymerized at 4°C may be attributed to the subsequent breakdown of the physical bonds formed during gelation. Although the described GelMA collapse is observed in both scaffolds without cell populations, it is important to note that matrix stiffening and contraction occurs because of ECM deposition in a 3D matrix. It has been

observed that MDAMB231 cells will secrete ECM and stiffen the matrix directly surrounding cells, resulting in localized contraction within the scaffold and subsequent matrix stiffening.[85] Therefore, we can expect scaffold collapse and contraction to have a direct impact on embedded cell populations, while ECM secretions from embedded cells will additionally affect the surrounding scaffolds. Both material and resident cell dependent effects on matrix contraction and stiffening must be considered when engineering 3D structures to best predict resolution and structural integrity of the desired geometry and application, particularly when using GelMA in 3D printing for tissue engineering.

Embedded spheroid outgrowth, sprouting, and proliferation is dependent on the material properties of GelMA (Figure 8). Spheroids embedded in matrices with the highest DS did not sprout into the surrounding matrix, and spheroids in the weakest matrix demonstrated no invasion. Spheroid invasion was observed in GelMA with storage moduli roughly between 400 and 1100 Pa. The most cell migration from the spheroid into the surrounding GelMA scaffold was observed with spheroids embedded in porcine GelMA with low DS polymerized at 37°C, which has a storage modulus (G') of on average of 723 Pa. Several publications report storage moduli greater than 5000 Pa, primarily in GelMA with concentrations greater than 10 wt%.[18, 20, 51, 86] Limited cell invasion was observed in piscine GelMA with low DS polymerized at 4°C with the lowest storage modulus (G') of 294 Pa. This is due to the low storage modulus (G') matrix lacking necessary structural integrity to support spheroid outgrowth. This observation suggests that there is an optimal window of material stiffnesses for spheroid outgrowth in GelMA, which is not a result of gelatin animal source. Therefore, gelatin animal source can be a tool to achieve a desired material stiffness, rather than a generalized matrix selected due to ambiguous chemical properties defined by amino acid compositions and available adhesion molecules. MDAMB231 spheroids proliferate into the surrounding scaffold when GelMA has storage moduli (G') between 400 to 800 Pa. Similar conclusions have previously been published, suggesting an optimal window of concentrations is present for melanoma spheroid cell invasion into collagen scaffolds.[87] This study reports matrices that are too soft lack structural integrity to support cell invasion, while cell migration is limited in stiff matrices due to high material density. Additionally, a study published by Berger *et al.* highlights that supplementing GelMA scaffolds with fibrous collagen is required for MDAMB231 spheroid invasion into scaffolds with storage moduli (G') higher than the optimal window identified herein.[84] Spheroid invasion was observed in composite GelMA-collagen scaffolds with storage moduli (G') as high as 12 kPa. This suggests spheroid invasion may be possible in GelMA scaffolds with coordinated physical gelation and chemical crosslinks upon supplementing the matrix with fibrous support materials, such as collagen.

Although the physical properties of high concentration GelMA often result in materials that are easier to process, improving printability for 3D printing and micropatterning applications, they are unlikely to support dynamic cell proliferation and spreading for embedded cell populations. Consideration of animal source, DS, and temperature at polymerization is critical to ensure desired response of embedded cells for tissue engineering and 3D printing applications.

CONCLUSIONS

Three-dimensional scaffolds are a key element of bioprinting and tissue engineering, providing a biomimetic or bioactive environment where cells exhibit *in vivo* characteristics. Popular scaffolds, such as Matrigel® and isolated collagen, are biocompatible, bioactive, and biodegradable, but are limited by small ranges of processing temperature, mechanical tunability, and available modification chemistries. Easily processible scaffolds, such as polyethylene glycol (PEG) and polysaccharide derivatives, natively lack bioactive components necessary for cell integration. GelMA offer both the desired bioactivity and tunable processing parameters to achieve the necessary material properties for micropatterning, printing, and 3D cell culture.

To contribute a guide for selection of GelMA synthesis and processing conditions, we have shown that animal source material of gelatin and the order of thermal processing steps affect the ultimate mechanical and functional properties of GelMA. This may be due to the method of hydrolysis, Bloom strength, molecular weight, and available primary amines. Gelation of gelatin can also be leveraged to achieve storage modulus (G') eight times higher than traditional crosslinked GelMA by coordinating physical gelation with chemical crosslinking. Coordinated physical gelation and chemical crosslinking can be used to pattern scaffolds to spatially align materials with different mechanical strengths but the same bulk chemical properties using photomasks. Even further, these scaffolds can be used to culture cell types that prefer stiffer surfaces with low concentration GelMA, therefore minimizing material requirements and avoiding possible solubility issues that may arise when attempting to achieve similar stiffnesses through adjusting concentration alone. Unfortunately, when not properly considered, this phenomenon also results in undesirable material outcomes. GelMA is increasing in popularity for 3D printing applications, particularly due to its biocompatibility, native groups for cell adhesion, and photocuring ability. Despite these advantages, GelMA often does not have the viscosity required for optimal bioprinting at concentrations that allow cell integration and proliferation. Many bioprinting companies recommend adjusting material properties by cooling GelMA, inducing gelation and therefore a 'more printable' material. This may account for variations in expected cellular interactions with the printed matrix due to an increase in final storage modulus (G') and molecular weight between crosslinks, as well as issues with repeatability in print quality. Our findings suggest more care needs to be taken when choosing GelMA animal source and polymerization temperature for tissue engineering applications, while also offering a new and exciting alternative to composite materials in applications where stiff scaffolds are desired.

EXPERIMENTAL METHODS

Gelatin Methacryloyl Synthesis:

GelMA was synthesized as previously reported.[47] Gelatin from porcine (Millipore Sigma, Type A, 300 g Bloom), bovine (Millipore Sigma, Type B, 225 g Bloom), or cold-water fish (Millipore Sigma) was dissolved in 1X PBS at 1 g gelatin per 10 mL 1X PBS at 60°C. After gelatin dissolved, temperature was cooled to 50°C and methacrylic anhydride (Millipore Sigma) was added per three reaction conditions. Briefly, these were defined by the ratio of

methacrylic anhydride to gram of gelatin: 750 μl·g^{-1}, 375 μl·g^{-1}, and 93.75 μl·g^{-1}. These reaction conditions and subsequent GelMA samples are referred to as 'High', 'Mid', and 'Low' degrees of substitution, respectively. The reaction was continued for 4 hours at 50°C. The reaction was stopped by adding equivalent volume of 1X PBS. The solution was dialyzed in distilled water using dialysis tubing with a molecular weight cutoff of 12-14 kDa (Spectrum) at 40°C for 7 days, with deionized water changed daily. GelMA was frozen at 80°C overnight and lyophilized for 5 days. The final product was stored at 4°C until use.

Colorimetric Detection of Primary Amines:

Methacrylation of GelMA was quantified by measuring the available primary amine groups with 2,4,6-trinitrobenzene sulfonic acid (TNBSA) (Millipore Sigma) after synthesis. GelMA, gelatin, and Bovine Serum Albumin (Millipore Sigma) were dissolved in 0.1 M sodium bicarbonate (VWR) at pH 8.5 at 400 μg·mL^{-1} and diluted to 200, 150, 100, 50, and 20 μg·mL^{-1} with 0.1 M sodium bicarbonate ($NaHCO_3$). Glycine (Millipore Sigma) was dissolved at 20 μg·mL^{-1} and diluted to 15, 10, 5, 2, and 0 μg·mL^{-1} with 0.1 M $NaHCO_3$. BSA and glycine were used as standard compounds for calculating the primary amine concentration. Each solution was tested in triplicate with 100 μL per well in a 96 well plate. TNBSA was diluted to 0.01% with 0.1 M $NaHCO_3$ and 50 μL was introduced to each well. Reaction continued for 2 hours at 37°C. Reaction was stopped by adding 50 μL of 10% sodium dodecyl sulfate in deionized H_2O and 25 μL 1 N HCl to each well. Absorbance was measured at 420 nm and 335 nm using a Biotek Synergy H1 microplate reader to determine available primary amines. Each tested condition was replicated (n = 9). Statistical analysis included t-test comparisons with a p-value of 0.05. Error bars are plotted as the standard deviation.

UV Rheological Analysis:

GelMA samples were prepared by first dissolving 0.5 wt% 2-Hydroxy-4′-(2-hydroxyethoxy)-2-methylpropiophenone photoinitiator (Millipore Sigma), also referred to as Irgacure 2959, in deionized water at 50°C. GelMA was dissolved at 5 wt% in Irgacure 2959 solution at 50°C. Some samples were incubated at 37°C prior to testing. Samples photocured after physical gelation were prepared by pipetting a 1 mL solution into a 20 mm diameter acrylic cylinder surrounded by tape and allowed to gel at 4°C for at least an hour. Piscine samples were not pipetted into a mold prior to testing due to lack of gelation. Crosslinking kinetics were determined using a TA Instruments Discovery Series Hybrid Rheometer HR-3 with the 365 nm UV LED accessory. Calibration was performed before use with a Silver Line radiometer. Measurements were collected with a 20 mm upper aluminum plate and a 20 mm acrylic bottom plate, allowing light to crosslink the GelMA samples from the UV LED accessory below. Liquid samples were tested with a gap size of 300 μm, gel samples were tested with a gap selected when a normal force was sensed with the loaded sample, between 1300 and 1500 μm. Samples were exposed to UV light at an intensity of 5 mW·cm^{-2} for 300 seconds, with a constant frequency of 1 Hz and strain at 1%. Storage modulus before and after UV polymerization for GelMA incubated at 4°C were determined by taking the initial and final values from the UV crosslinking kinetics data (Figure 4d–f). After polymerization, a frequency sweep was performed from 0.1 Hz to 10 Hz at 1% strain. Storage moduli measurements were compared between samples crosslinked after incubation at 37°C and

4°C by averaging modulus across the frequency sweep (Figure 4a–c). Curing points were determined by calculating the second derivative of the storage modulus (G') curve during polymerization. Gel points were determined by determining when tan(δ) = 1. For data that did not have a crossover point, gel point was identified when tan(δ) is at a maximum. All measurements were collected at ambient room temperature, though tested immediately after removing from incubation temperature. All measurements were completed in triplicate (n = 3). Statistical analysis included *t*-test comparisons with a p-value of 0.05. Error bars are plotted as the standard deviation.

Temperature Sweep Rheological Analysis:

Porcine GelMA samples were prepared at 5 wt% with 0.5 wt% Irgacure 2959 in a 6 well plate, with 2 mL unpolymerized GelMA introduced in each well. Samples were polymerized for 5 minutes with a UV lamp (Dymax) at 10 $mW \cdot cm^{-2}$. GelMA samples were polymerized after at least an hour of equilibration at either 37°C or 4°C. Temperature sweeps were collected using StressTech Rheometer (ATS Rheosystems) with a Peltier plate temperature system and 20 mm serrated parallel plate accessory. Measurements were made by holding strain and frequency constant at 5% and 1 Hz, respectively, and sweeping temperature from 50 °C to 4 °C. Samples equilibrated at the initial temperature for 5 minutes prior to testing and equilibrated at each set temperature for 60 seconds. All measurements were completed in triplicate. Error bars are plotted as the standard deviation.

Swelling Characterization:

GelMA was dissolved at 6 wt% with 0.5 wt% Irgacure 2929 in deionized H_2O at 50 °C. GelMA solution was added to each well of a 12 well plate at 1 mL per well and incubated at 4°C or 37°C for at least 1 hour. Cooled samples were photocured on ice for 180 seconds at 10 $mW \cdot cm^{-2}$. Heated samples were photocured for 180 seconds at 10 $mW \cdot cm^{-2}$. Deionized H_2O was added to each well and incubated for 24 hours at 37 °C to remove uncrosslinked material and reach equilibrium water content. Samples were removed from PBS, blotted with an absorbent pad, and weighed using an analytical balance. Samples were frozen samples overnight at −80 °C and lyophilized for 24 hours. They were then weighed again using an analytical balance. Each condition was testing in triplicate. Statistical analysis included t-test comparisons with a p-value of 0.05. Error bars are plotted as the standard deviation.

Cell Growth on GelMA:

GelMA was cured between sterile PDMS and a glass coverslip, using #1 glass coverslips as spacers to achieve gel thickness of approximately 150 μm. High DS GelMA and photoinitiator was dissolved in 1X sterile PBS at 4 wt% and 0.5 wt%, respectively. Just 25 μL GelMA solution was pipetted between PDMS and coverslip, with coverslip spacers, and chilled for 15 minutes at 4°C to allow gelation. Using a photomask on transparency paper, gels were patterned at an intensity of 60 $mW \cdot cm^{-2}$ for 60 seconds. Gels were then heated to 50°C for 5 minutes, and then flood exposed to UV without the mask for 60 seconds at 60 $mW \cdot cm^{-2}$. Gels were covered in Dulbecco's Modified Eagle Medium (DMEM) with 10% fetal bovine serum and 1X penicillin/streptomycin solution in a 37°C incubator with 5% CO_2 and 100% humidity prior to cell seeding. The same protocol was followed for un-

patterned gels, with only the heating or cooling step prior to flood UV exposure. Human neonatal Dermal Fibroblasts (HDFn) (Lonza) were cultured per standard protocol with DMEM with 10% fetal bovine serum and 1X penicillin/streptomycin solution in a 37°C incubator with 5% CO_2 and 100% humidity. Cells were trypsinized and seeded on top of gels at a density of 50,000 cells mL^{-1} in a 6-well plate. After 24 hours of culture, cells were fixed with 4 wt% paraformaldehyde, permeabilized with 0.5 v/v% Triton-X and blocked with 2 wt% bovine serum albumin. Cells were stained with phalloidin-iFluor488 (Abcam) and DAPI, and they were imaged using a Zeiss LSM 710 confocal microscope. Aspect ratio values were determined using ImageJ software. A threshold was applied to all images and then the 'Measure particle' function was used to define cell outlines. Aspect ratio measurements are defined as the longest distance of the cell divided by the shortest distance. Cells were analyzed at $n \geq 55$, imaged from 40X magnification. Statistical analysis included t-test comparisons with a p-value of 0.05. Error bars are plotted as the standard deviation.

Spheroid Culture and Quantification:

MDAMB231 spheroids were created using the liquid overlay technique described previously.[88] In short, MDAMB231 mammary cancer cells (ATCC) were cultured in DMEM with 10 % fetal bovine serum and 1X penicillin/streptomycin solution. Round bottom, cell-repellant 96 well plates were seeded with 100 μL suspension solution with 10,000 MDAMB231 cells. Suspension solution consisted of cell medium supplemented with 3.5 w/v% Matrigel®. Cells were cultured for 3 days in a 5% CO_2, 100% humidity incubator at 37°C. After the culture period, spheroids were removed from the well plate, pooled, centrifuged to produce a pellet, and washed with cell medium. Spheroids were suspended at a concentration of 1 spheroid per 25 μL media. GelMA was dissolved in phosphate buffered saline at 10 wt% with 1 wt% Irgacure photoinitiator. GelMA solution was combined with spheroid solution at a 1:1 ratio to achieve 1 spheroid per 50 μL solution containing 5 wt% GelMA with 0.5 wt% photoinitiator. GelMA solutions containing spheroids were pipetted into single wells of a 16-well chamber slide or 96-well plate at 75 μL per well to achieve at least one spheroid per well. GelMA solutions were polymerized at an UV intensity of 10 $mW \cdot cm^{-2}$ for 120 seconds. The GelMA samples containing spheroids were covered with 100 μL cell medium. Medium was replaced every 48 hours after seeding. After 4 days of culture, spheroid viability was tested by adding calcein AM and ethidium homodimer-1 to each well to achieve a final concentration of 2 μM and 4 μM, respectively. Cells were incubated for 1 hour at 37°C. Images were collected using a Nikon TE 2000E inverted fluorescent microscope with a mechanical stage, and Micro-manager software. [89] Spheroids were imaged to observe morphology and sprouting by first fixing with 4% paraformaldehyde for 30 minutes, followed by permeabilization with 0.5 v/v% Triton-X for 10 minutes. Cells were stained with phalloidin-iFluor488 (Abcam) and DAPI and imaged using a Zeiss LSM 710 confocal microscope. Fifty z-stack imaged were collected of each spheroid, and max projected for analysis. Spheroid size was determined from fluorescent images manually using ImageJ software. Quantification of brightfield images was also achieved using ImageJ software. The 'Find Edges' function was used to determine edges of spheroids, and then a profile plot of the normalized integrated intensities from the center of the spheroid was calculated using the Radial Profile plugin. Statistical analysis included t-

test comparisons with a p-value of 0.05. Error bars are plotted as the standard deviation. Spheroids were analyzed at $n \geq 3$.

GelMA Contraction:

GelMA and photoinitiator was dissolved in 1X PBS at 5 wt% and 0.5 wt%, respectively. Solutions were pipetted into a 96 well plate at 100 μL per well and polymerized after incubation for 25 minutes at 37°C and 4°C. Additional 1X PBS was added on top of polymerized GelMA at 100 μL per well and incubated at room temperature for 44 hours followed by a 27 hour incubation at 37°C. Diameter was measured by taking brightfield images using a Nikon TE 2000E inverted fluorescent microscope with a 1X objective, and quantifying with ImageJ software. Samples were tested in triplicate. Statistical analysis included t-test comparisons with a p-value of 0.05.

Supplementary Material

Refer to Web version on PubMed Central for supplementary material.

ACKNOWLEDGEMENTS

The authors would like to thank Dr. Saad Kahn and the NC State Food Rheology Lab for generously allowing us to use their rheometers. This work was supported in part by American Heart Association Grant 18TPA34230031. A.T.Y was supported by the Pre-doctoral Training Program in Integrative Vascular Biology at the University of North Carolina at Chapel Hill (NIH 2T32HL069768-16). O.C.W. was supported by the National Science Foundation (EEC1160483) through the NSF Nanosystems Engineering Research Center (NERC) for Advanced Self-Powered Systems of Integrated Sensors and Technologies (ASSIST).

REFERENCES

1. Frantz C; Stewart KM; Weaver VM, The extracellular matrix at a glance. J Cell Sci 2010, 123 (Pt 24), 4195–4200. [PubMed: 21123617]
2. Starborg T; Kalson NS; Lu Y; Mironov A; Cootes TF; Holmes DF; Kadler KE, Using transmission electron microscopy and 3View to determine collagen fibril size and three-dimensional organization. Nature Protocols 2013, 8 (7), 1433–1448. [PubMed: 23807286]
3. Parry DAD; Barnes GRG; Craig AS; Phillips DC, A comparison of the size distribution of collagen fibrils in connective tissues as a function of age and a possible relation between fibril size distribution and mechanical properties. Proceedings of the Royal Society of London. Series B. Biological Sciences 1978, 203 (1152), 305–321.
4. Shoulders MD; Raines RT, Collagen structure and stability. Annu Rev Biochem 2009, 78, 929–58. [PubMed: 19344236]
5. Ali MY; Chuang CY; Saif MT, Reprogramming cellular phenotype by soft collagen gels. Soft Matter 2014, 10 (44), 8829–37. [PubMed: 25284029]
6. Hansen LK; Wilhelm J; Fassett JT, Regulation of hepatocyte cell cycle progression and differentiation by type I collagen structure. Curr Top Dev Biol 2006, 72, 205–36. [PubMed: 16564336]
7. Shi S; Kirk M; Kahn AJ, The role of type I collagen in the regulation of the osteoblast phenotype. J Bone Miner Res 1996, 11 (8), 1139–45. [PubMed: 8854250]
8. Garcia AJ; Reyes CD, Bio-adhesive surfaces to promote osteoblast differentiation and bone formation. J Dent Res 2005, 84 (5), 407–13. [PubMed: 15840774]
9. Engler AJ; Sen S; Sweeney HL; Discher DE, Matrix elasticity directs stem cell lineage specification. Cell 2006, 126 (4), 677–89. [PubMed: 16923388]

10. Engler AJ; Griffin MA; Sen S; Bonnemann CG; Sweeney HL; Discher DE, Myotubes differentiate optimally on substrates with tissue-like stiffness: pathological implications for soft or stiff microenvironments. J Cell Biol 2004, 166 (6), 877–87. [PubMed: 15364962]
11. Gallop PM; Paz MA, Posttranslational protein modifications, with special attention to collagen and elastin. Physiol Rev 1975, 55 (3), 418–87. [PubMed: 50603]
12. Copes F; Pien N; Van Vlierberghe S; Boccafoschi F; Mantovani D, Collagen-Based Tissue Engineering Strategies for Vascular Medicine. Front Bioeng Biotechnol 2019, 7, 166. [PubMed: 31355194]
13. Rýglová Š; Braun M; Suchý T, Collagen and Its Modifications—Crucial Aspects with Concern to Its Processing and Analysis. Macromolecular Materials and Engineering 2017, 302 (6), 1600460.
14. Gu L; Shan T; Ma Y.-x.; Tay FR; Niu L, Novel Biomedical Applications of Crosslinked Collagen. Trends in Biotechnology 2019, 37 (5), 464–491. [PubMed: 30447877]
15. Djagny VB; Wang Z; Xu S, Gelatin: a valuable protein for food and pharmaceutical industries: review. Crit Rev Food Sci Nutr 2001, 41 (6), 481–92. [PubMed: 11592686]
16. Yue K; Trujillo-de Santiago G; Alvarez MM; Tamayol A; Annabi N; Khademhosseini A, Synthesis, properties, and biomedical applications of gelatin methacryloyl (GelMA) hydrogels. Biomaterials 2015, 73, 254–71. [PubMed: 26414409]
17. Nichol JW; Koshy ST; Bae H; Hwang CM; Yamanlar S; Khademhosseini A, Cell-laden microengineered gelatin methacrylate hydrogels. Biomaterials 2010, 31 (21), 5536–5544. [PubMed: 20417964]
18. Van den Bulcke AI; Bogdanov B; De Rooze N; Schacht EH; Cornelissen M; Berghmans H, Structural and rheological properties of methacrylamide modified gelatin hydrogels. Biomacromolecules 2000, 1 (1), 31–38. [PubMed: 11709840]
19. Pepelanova I; Kruppa K; Scheper T; Lavrentieva A, Gelatin-Methacryloyl (GelMA) hydrogels with defined degree of functionalization as a versatile toolkit for 3D cell culture and extrusion bioprinting. Bioengineering 2018, 5 (3), 55.
20. O'Connell CD; Zhang B; Onofrillo C; Duchi S; Blanchard R; Quigley A; Bourke J; Gambhir S; Kapsa R; Di Bella C; Choong P; Wallace GG, Tailoring the mechanical properties of gelatin methacryloyl hydrogels through manipulation of the photocrosslinking conditions. Soft Matter 2018, 14 (11), 2142–2151. [PubMed: 29488996]
21. Chen YC; Lin RZ; Qi H; Yang YZ; Bae HJ; Melero-Martin JM; Khademhosseini A, Functional Human Vascular Network Generated in Photocrosslinkable Gelatin Methacrylate Hydrogels. Adv Funct Mater 2012, 22 (10), 2027–2039. [PubMed: 22907987]
22. Lee BH; Lum N; Seow LY; Lim PQ; Tan LP, Synthesis and Characterization of Types A and B Gelatin Methacryloyl for Bioink Applications. Materials 2016, 9 (10).
23. Wang ZJ; Tian ZL; Menard F; Kim K, Comparative study of gelatin methacrylate hydrogels from different sources for biofabrication applications. Biofabrication 2017, 9 (4).
24. Yang XJ; Zheng PJ; Cui Z; Zhao NQ; Wang YF; Yao KD, Swelling behaviour and elastic properties of gelatin gels. Polymer International 1997, 44 (4), 4.
25. Zaupa A; Byres N; Dal Zovo C; Acevedo CA; Angelopoulos I; Terraza C; Nestle N; Abarzua-Illanes PN; Quero F; Diaz-Calderon P; Olguin Y; Akentjew TL; Wilkens CA; Padilla C; Zacconi FC; Pino-Lagos K; Blaker JJ; Khoury M; Enrione J; Acevedo JP, Cold-adaptation of a methacrylamide gelatin towards the expansion of the biomaterial toolbox for specialized functionalities in tissue engineering. Mater Sci Eng C Mater Biol Appl 2019, 102, 373–390. [PubMed: 31147009]
26. Yoon HJ; Shin SR; Cha JM; Lee SH; Kim JH; Do JT; Song H; Bae H, Cold Water Fish Gelatin Methacryloyl Hydrogel for Tissue Engineering Application. PLoS One 2016, 11 (10), e0163902. [PubMed: 27723807]
27. Haug IJ; Draget KI; Smidsrod O, Physical and rheological properties of fish gelatin compared to mammalian gelatin. Food Hydrocolloids 2004, 18 (2), 10.
28. Raja Nhari RMH; Yaakob C; A I; A N, Chemical and functional properties of bovine and porcine skin gelatin. International Food Research Journal 2011, 18, 787–791.
29. Gorgieva S; Kokol V, Collagen-vs. Gelatine-Based Biomaterials and Their Biocompatibility: Review and Perspectives. Biomaterials Applications for Nanomedicine 2011, 17–52.

30. Karim A; Bhat R, Fish gelatin: properties, challenges, and prospects as an alternative to mammalian gelatins. Food hydrocolloids 2009, 23 (3), 563–576.
31. Alfaro A; Balbinot E; Weber C; Tonial I; Machado A, Fish Gelatin: Characteristics, Functional Properties, Applications and Future Potentials. Food Engineering Reviews 2014, 7, 33–44.
32. Guo L; Colby RH; Lusignan CP; Howe AM, Physical gelation of gelatin studied with rheo-optics. Macromolecules 2003, 36 (26), 10009–10020.
33. Panouillé M; Larreta-Garde V, Gelation behaviour of gelatin and alginate mixtures. Food hydrocolloids 2009, 23 (4), 1074–1080.
34. Hayashi A; Oh SC, Gelation of Gelatin Solution. Agr Biol Chem Tokyo 1983, 47 (8), 1711–1716.
35. Krishnamoorthy S; Noorani B; Xu C, Effects of Encapsulated Cells on the Physical-Mechanical Properties and Microstructure of Gelatin Methacrylate Hydrogels. Int J Mol Sci 2019, 20 (20).
36. Yin J; Yan ML; Wang YC; Fu JZ; Suo HR, 3D Bioprinting of Low-Concentration Cell-Laden Gelatin Methacrylate (GelMA) Bioinks with a Two-Step Cross-linking Strategy. Acs Appl Mater Inter 2018, 10 (8), 6849–6857.
37. Sun M; Sun X; Wang Z; Guo S; Yu G; Yang H, Synthesis and Properties of Gelatin Methacryloyl (GelMA) Hydrogels and Their Recent Applications in Load-Bearing Tissue. Polymers (Basel) 2018, 10 (11).
38. Sewald L; Claassen C; Gotz T; Claassen MH; Truffault V; Tovar GEM; Southan A; Borchers K, Beyond the Modification Degree: Impact of Raw Material on Physicochemical Properties of Gelatin Type A and Type B Methacryloyls. Macromol Biosci 2018, 18 (12), e1800168. [PubMed: 30286274]
39. Rizwan M; Peh GSL; Ang HP; Lwin NC; Adnan K; Mehta JS; Tan WS; Yim EKF, Sequentially-crosslinked bioactive hydrogels as nano-patterned substrates with customizable stiffness and degradation for corneal tissue engineering applications. Biomaterials 2017, 120, 139–154. [PubMed: 28061402]
40. Jiang J; Liu A; Chen C; Tang J; Fan H; Sun J; Fan H, An efficient two-step preparation of photocrosslinked gelatin microspheres as cell carriers to support MC3T3-E1 cells osteogenic performance. Colloids and Surfaces B: Biointerfaces 2020, 188, 110798. [PubMed: 31955020]
41. Park HE; Gasek N; Hwang J; Weiss DJ; Lee PC, Effect of temperature on gelation and cross-linking of gelatin methacryloyl for biomedical applications. Physics of Fluids 2020, 32 (3), 033102.
42. Kim P; Yuan A; Nam KH; Jiao A; Kim DH, Fabrication of poly(ethylene glycol): gelatin methacrylate composite nanostructures with tunable stiffness and degradation for vascular tissue engineering. Biofabrication 2014, 6 (2).
43. Shin SR; Aghaei-Ghareh-Bolagh B; Dang TT; Topkaya SN; Gao XG; Yang SY; Jung SM; Oh JH; Dokmeci MR; Tang XW; Khademhosseini A, Cell-laden Microengineered and Mechanically Tunable Hybrid Hydrogels of Gelatin and Graphene Oxide. Adv Mater 2013, 25 (44), 6385–6391. [PubMed: 23996513]
44. Zhu K; Chen N; Liu X; Mu X; Zhang WJ; Wang CS; Zhang YS, A General Strategy for Extrusion Bioprinting of Bio-Macromolecular Bioinks through Alginate-Templated Dual-Stage Crosslinking. Macromol Biosci 2018, 18 (9).
45. Zheng JF; Zhao FJ; Zhang W; Mo YF; Zeng L; Li X; Chen XF, Sequentially-crosslinked biomimetic bioactive glass/gelatin methacryloyl composites hydrogels for bone regeneration. Mat Sci Eng C-Mater 2018, 89, 119–127.
46. Krishnamoorthy S; Zhang ZY; Xu CX, Biofabrication of three-dimensional cellular structures based on gelatin methacrylate-alginate interpenetrating network hydrogel. J Biomater Appl 2019, 33 (8), 1105–1117. [PubMed: 30636494]
47. Daniele MA; Adams AA; Naciri J; North SH; Ligler FS, Interpenetrating networks based on gelatin methacrylamide and PEG formed using concurrent thiol click chemistries for hydrogel tissue engineering scaffolds. Biomaterials 2014, 35 (6), 1845–1856. [PubMed: 24314597]
48. Haug IJ; Draget KI, 6 - Gelatin In Handbook of Hydrocolloids (Second Edition), Phillips GO; Williams PA, Eds. Woodhead Publishing: 2009; pp 142–163.

49. Stevenson AT; Jankus DJ; Tarshis MA; Whittington AR, The correlation between gelatin macroscale differences and nanoparticle properties: providing insight into biopolymer variability. Nanoscale 2018, 10 (21), 10094–10108. [PubMed: 29780985]
50. Shirahama H; Lee BH; Tan LP; Cho NJ, Precise Tuning of Facile One-Pot Gelatin Methacryloyl (GelMA) Synthesis. Sci Rep 2016, 6, 31036. [PubMed: 27503340]
51. Lee BH; Lum N; Seow LY; Lim PQ; Tan LP, Synthesis and Characterization of Types A and B Gelatin Methacryloyl for Bioink Applications. Materials (Basel) 2016, 9 (10).
52. Celikkin N; Mastrogiacomo S; Jaroszewicz J; Walboomers XF; Swieszkowski W, Gelatin methacrylate scaffold for bone tissue engineering: The influence of polymer concentration. J Biomed Mater Res A 2018, 106 (1), 201–209. [PubMed: 28884519]
53. Shin SR; Bae H; Cha JM; Mun JY; Chen Y-C; Tekin H; Shin H; Farshchi S; Dokmeci MR; Tang S; Khademhosseini A, Carbon Nanotube Reinforced Hybrid Microgels as Scaffold Materials for Cell Encapsulation. ACS Nano 2012, 6 (1), 362–372. [PubMed: 22117858]
54. Shin SR; Aghaei-Ghareh-Bolagh B; Dang TT; Topkaya SN; Gao X; Yang SY; Jung SM; Oh JH; Dokmeci MR; Tang X; Khademhosseini A, Cell-laden Microengineered and Mechanically Tunable Hybrid Hydrogels of Gelatin and Graphene Oxide. Adv Mater 2013, 25 (44), 6385–6391. [PubMed: 23996513]
55. Zheng J; Zhu M; Ferracci G; Cho N-J; Lee BH, Hydrolytic Stability of Methacrylamide and Methacrylate in Gelatin Methacryloyl and Decoupling of Gelatin Methacrylamide from Gelatin Methacryloyl through Hydrolysis. Macromolecular Chemistry and Physics 2018, 219 (18), 1800266.
56. Yue K; Li X; Schrobback K; Sheikhi A; Annabi N; Leijten J; Zhang W; Zhang YS; Hutmacher DW; Klein TJ; Khademhosseini A, Structural analysis of photocrosslinkable methacryloyl-modified protein derivatives. Biomaterials 2017, 139, 163–171. [PubMed: 28618346]
57. Caliari SR; Burdick JA, A practical guide to hydrogels for cell culture. Nat Methods 2016, 13 (5), 405–14. [PubMed: 27123816]
58. Ehrbar M; Sala A; Lienemann P; Ranga A; Mosiewicz K; Bittermann A; Rizzi SC; Weber FE; Lutolf MP, Elucidating the role of matrix stiffness in 3D cell migration and remodeling. Biophys J 2011, 100 (2), 284–93. [PubMed: 21244824]
59. Henderson G Jr; Campbell D; Kuzmicz V; Sperling L, Gelatin as a physically crosslinked elastomer. Journal of Chemical Education 1985, 62 (3), 269.
60. Kulisiewicz L; Baars A; Delgado A, Effect of high hydrostatic pressure on structure of gelatin gels. Technical Sciences 2007, 55 (2).
61. Oakenfull D; Scott A, Gelatin gels in deuterium oxide. Food Hydrocolloids 2003, 17 (2), 207–210.
62. Wisotzki EI; Hennes M; Schuldt C; Engert F; Knolle W; Decker U; Käs JA; Zink M; Mayr SG, Tailoring the material properties of gelatin hydrogels by high energy electron irradiation. Journal of Materials Chemistry B 2014, 2 (27), 4297–4309. [PubMed: 32261568]
63. Deiber JA; Ottone ML; Piaggio MV; Peirotti MB, Characterization of cross-linked polyampholytic gelatin hydrogels through the rubber elasticity and thermodynamic swelling theories. Polymer 2009, 50 (25), 6065–6075.
64. Billiet T; Van Gasse B; Gevaert E; Cornelissen M; Martins JC; Dubruel P, Quantitative contrasts in the photopolymerization of acrylamide and methacrylamide-functionalized gelatin hydrogel building blocks. Macromol Biosci 2013, 13 (11), 1531–45. [PubMed: 24000135]
65. Lee KY; Rowley JA; Eiselt P; Moy EM; Bouhadir KH; Mooney DJ, Controlling Mechanical and Swelling Properties of Alginate Hydrogels Independently by Cross-Linker Type and Cross-Linking Density. Macromolecules 2000, 33 (11), 4291–4294.
66. Cox TR; Erler JT, Remodeling and homeostasis of the extracellular matrix: implications for fibrotic diseases and cancer. Dis Model Mech 2011, 4 (2), 165–178. [PubMed: 21324931]
67. Handorf AM; Zhou YX; Halanski MA; Li WJ, Tissue Stiffness Dictates Development, Homeostasis, and Disease Progression. Organogenesis 2015, 11 (1), 1–15. [PubMed: 25915734]
68. Hopp I; Michelmore A; Smith LE; Robinson DE; Bachhuka A; Mierczynska A; Vasilev K, The influence of substrate stiffness gradients on primary human dermal fibroblasts. Biomaterials 2013, 34 (21), 5070–5077. [PubMed: 23587444]

69. Lo CM; Wang HB; Dembo M; Wang YL, Cell movement is guided by the rigidity of the substrate. Biophys J 2000, 79 (1), 144–152. [PubMed: 10866943]

70. Dokukina IV; Gracheva ME, A Model of Fibroblast Motility on Substrates with Different Rigidities. Biophys J 2010, 98 (12), 2794–2803. [PubMed: 20550891]

71. Xie M; Gao Q; Zhao H; Nie J; Fu Z; Wang H; Chen L; Shao L; Fu J; Chen Z; He Y, Electro-Assisted Bioprinting of Low-Concentration GelMA Microdroplets. Small 2019, 15 (4), e1804216. [PubMed: 30569632]

72. Ding HZ; Illsley NP; Chang RC, 3D Bioprinted GelMA Based Models for the Study of Trophoblast Cell Invasion. Sci Rep-Uk 2019, 9.

73. Yin J; Yan M; Wang Y; Fu J; Suo H, 3D bioprinting of low concentration cell-laden gelatin methacrylate (GelMA) bioinks with two-step crosslinking strategy. ACS Appl Mater Interfaces 2018.

74. Costantini M; Testa S; Fornetti E; Barbetta A; Trombetta M; Cannata S; Gargioli C; Rainer A, Engineering muscle networks in 3D GelMA hydrogels: influence of mechanical stiffness and geometrical confinement. Front Bioeng Biotech 2017.

75. Munoz Z; Shi H; Lin CC, Gelatin hydrogels formed by orthogonal thiol–norbornene photochemistry for cell encapsulation. Biomater Sci-Uk 2014, 2 (8), 9.

76. Tenje M; Cantoni F; Porras Hernández AM; Searle SS; Johansson S; Barbe L; Antfolk M; Pohlit H, A practical guide to microfabrication and patterning of hydrogels for biomimetic cell culture scaffolds. Organs-on-a-Chip 2020, 2, 100003.

77. Khetan S; Burdick JA, Patterning network structure to spatially control cellular remodeling and stem cell fate within 3-dimensional hydrogels. Biomaterials 2010, 31 (32), 8228–8234. [PubMed: 20674004]

78. Baker BM; Chen CS, Deconstructing the third dimension – how 3D culture microenvironments alter cellular cues. J Cell Sci 2012, 125 (13), 3015. [PubMed: 22797912]

79. Berger AJ; Linsmeier KM; Kreeger PK; Masters KS, Decoupling the effects of stiffness and fiber density on cellular behaviors via an interpenetrating network of gelatin-methacrylate and collagen. Biomaterials 2017, 141, 125–135. [PubMed: 28683337]

80. Carey SP; Martin KE; Reinhart-King CA, Three-dimensional collagen matrix induces a mechanosensitive invasive epithelial phenotype. Sci Rep 2017, 7, 42088. [PubMed: 28186196]

81. Dolega ME; Delarue M; Ingremeau F; Prost J; Delon A; Cappello G, Cell-like pressure sensors reveal increase of mechanical stress towards the core of multicellular spheroids under compression. Nat Commun 2017, 8. [PubMed: 28364116]

82. Delarue M; Monte F; Vignjevic D; Prost J; Joanny JF; Cappello G, Compressive Stress Inhibits Proliferation in Tumor Spheroids through a Volume Limitation. Biophys J 2014, 107 (8), 1821–1828. [PubMed: 25418163]

83. Helmlinger G; Netti PA; Lichtenbeld HC; Melder RJ; Jain RK, Solid stress inhibits the growth of multicellular tumor spheroids. Nat Biotechnol 1997, 15 (8), 778–783. [PubMed: 9255794]

84. Taubenberger AV; Girardo S; Traber N; Fischer-Friedrich E; Krater M; Wagner K; Kurth T; Richter I; Haller B; Binner M; Hahn D; Freudenberg U; Werner C; Guck J, 3D Microenvironment Stiffness Regulates Tumor Spheroid Growth and Mechanics via p21 and ROCK. Adv Biosyst 2019, 3 (9).

85. Han YL; Ronceray P; Xu G; Malandrino A; Kamm RD; Lenz M; Broedersz CP; Guo M, Cell contraction induces long-ranged stress stiffening in the extracellular matrix. Proceedings of the National Academy of Sciences 2018, 115 (16), 4075.

86. Zhu M; Wang Y; Ferracci G; Zheng J; Cho NJ; Lee BH, Gelatin methacryloyl and its hydrogels with an exceptional degree of controllability and batch-to-batch consistency. Sci Rep 2019, 9 (1), 6863. [PubMed: 31053756]

87. Ahmadzadeh H; Webster MR; Behera R; Jimenez Valencia AM; Wirtz D; Weeraratna AT; Shenoy VB, Modeling the two-way feedback between contractility and matrix realignment reveals a nonlinear mode of cancer cell invasion. Proceedings of the National Academy of Sciences 2017, 114 (9), E1617.

88. Froehlich K; Haeger JD; Heger J; Pastuschek J; Photini SM; Yan Y; Lupp A; Pfarrer C; Mrowka R; Schleussner E; Markert UR; Schmidt A, Generation of Multicellular Breast Cancer Tumor

Spheroids: Comparison of Different Protocols. J Mammary Gland Biol Neoplasia 2016, 21 (3–4), 89–98. [PubMed: 27518775]

89. Edelstein AD; Tsuchida MA; Amodaj N; Pinkard H; Vale RD; Stuurman N, Advanced methods of microscope control using microManager software. Journal of Biological Methods 2014, 1 (2), e10. [PubMed: 25606571]

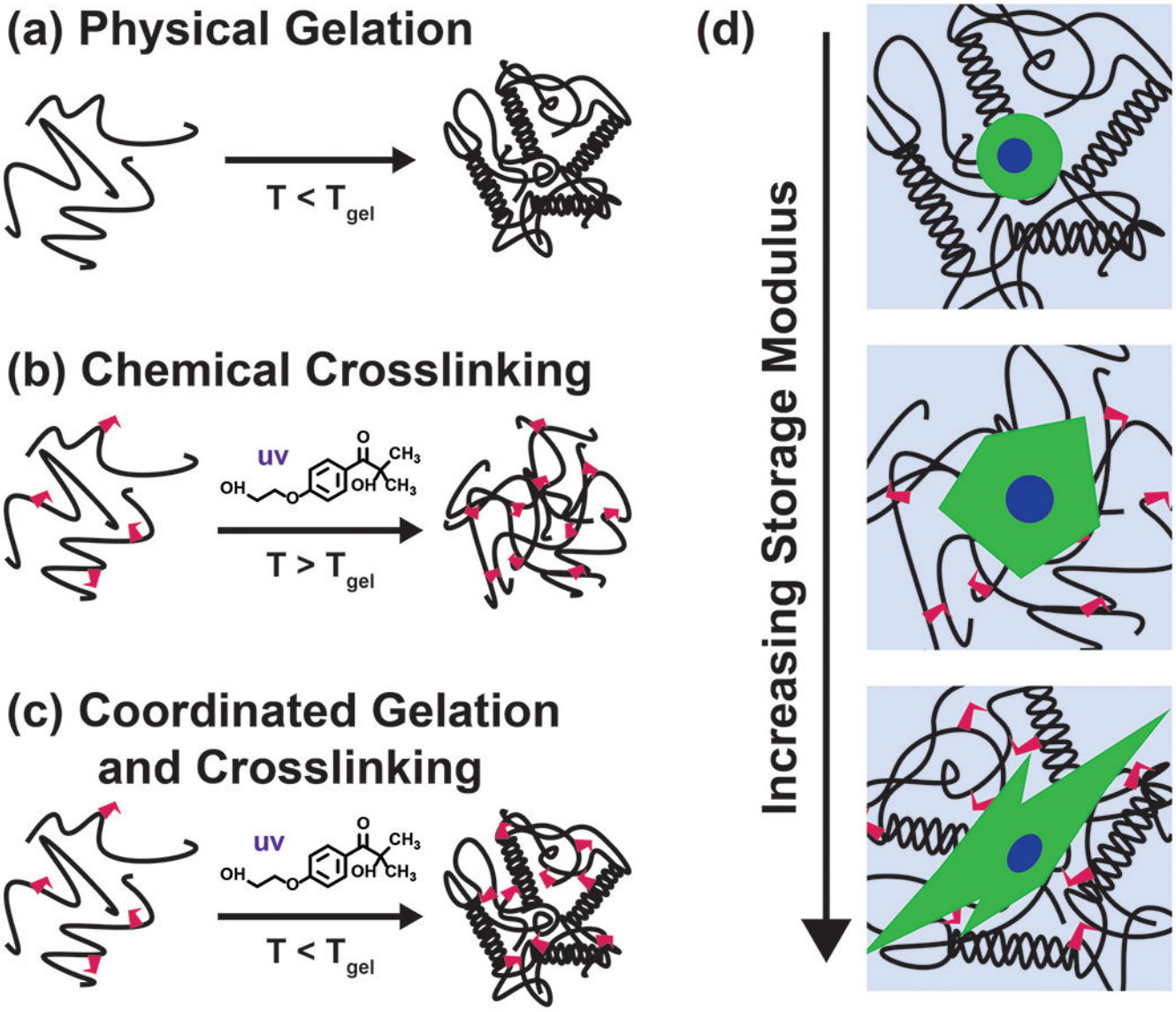

Figure 1.

GelMA undergoes (a) only chemical gelation via crosslinking in the presence of Irgacure 2959 photoinitiator and UV light above the thermal gel point, (b) only physical gelation when cooled below the gel point, and (c) coordinated physical gelation and chemical gelation via crosslinking when cooled below the gel point and exposed to UV light in the presence of Irgacure 2959 photoinitiator. (d) Adherent cells undergo morphological changes depending on the GelMA crosslinking method and subsequent scaffold stiffness.

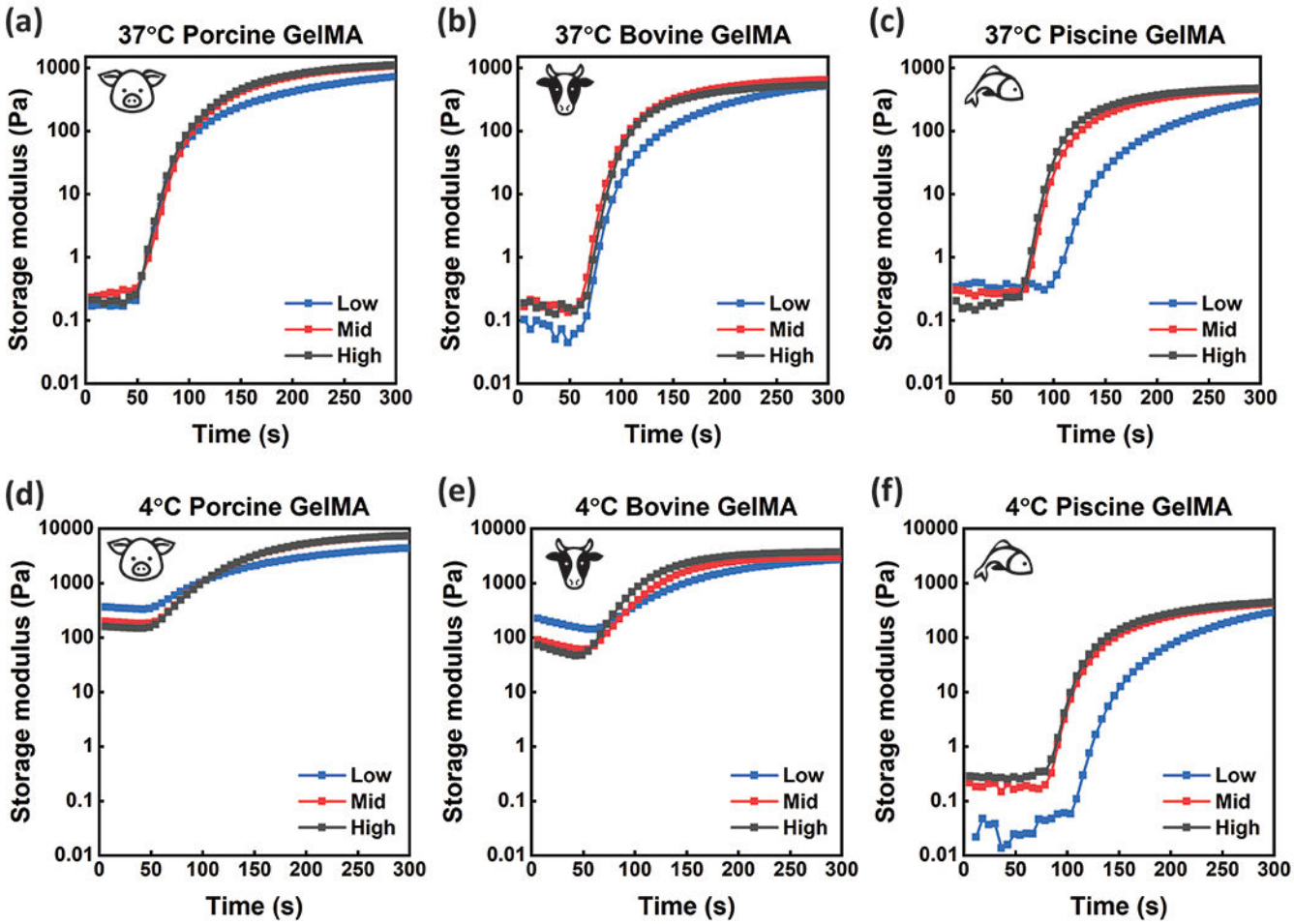

Figure 2.

GelMA synthesized from (a) porcine gelatin, (b) bovine gelatin, and (c) cold-water fish gelatin was photo-cross-linked (λ =365 nm) on a parallel plate rheometer at room temperature with 5mW·cm^{-2} intensity for 5 minutes after incubation at 37°C to determine crosslinking kinetics. GelMA synthesized from (d) porcine gelatin, (e) bovine gelatin, and (f) cold-water fish gelatin was photo-crosslinked (λ =365 nm) with the same testing parameters after incubation at 4°C to determine crosslinking kinetics of materials with both physical and chemical crosslinks. GelMA samples were tested at high, mid, and low DS. Data represents the average Storage modulus (G') across three replicates.

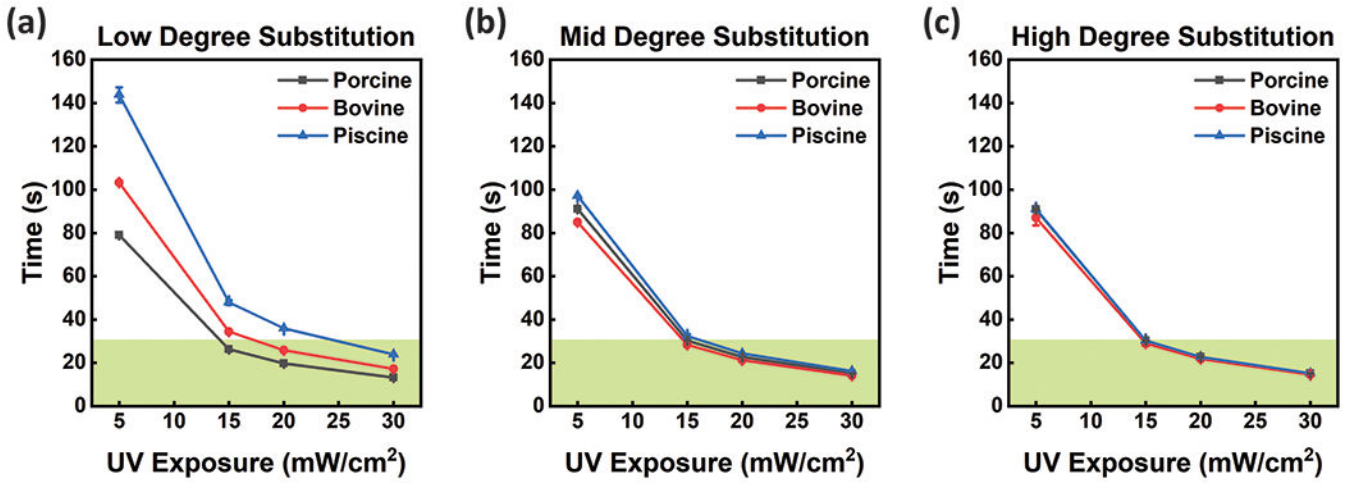

Figure 3.

Cure points for GelMA synthesized from different animal sources and (a) low, (b) mid, and (c) high degrees of substitution were determined based on crosslinking kinetics. Cure points were used to determine polymerization times with different UV intensities for all conditions, useful for defining printability of each material. The green region highlights cure points that require less than 30 seconds of UV Exposure, a metric important for 'bioprintability' and micropatterning. Error bars are plotted as the standard deviation (n≥3).

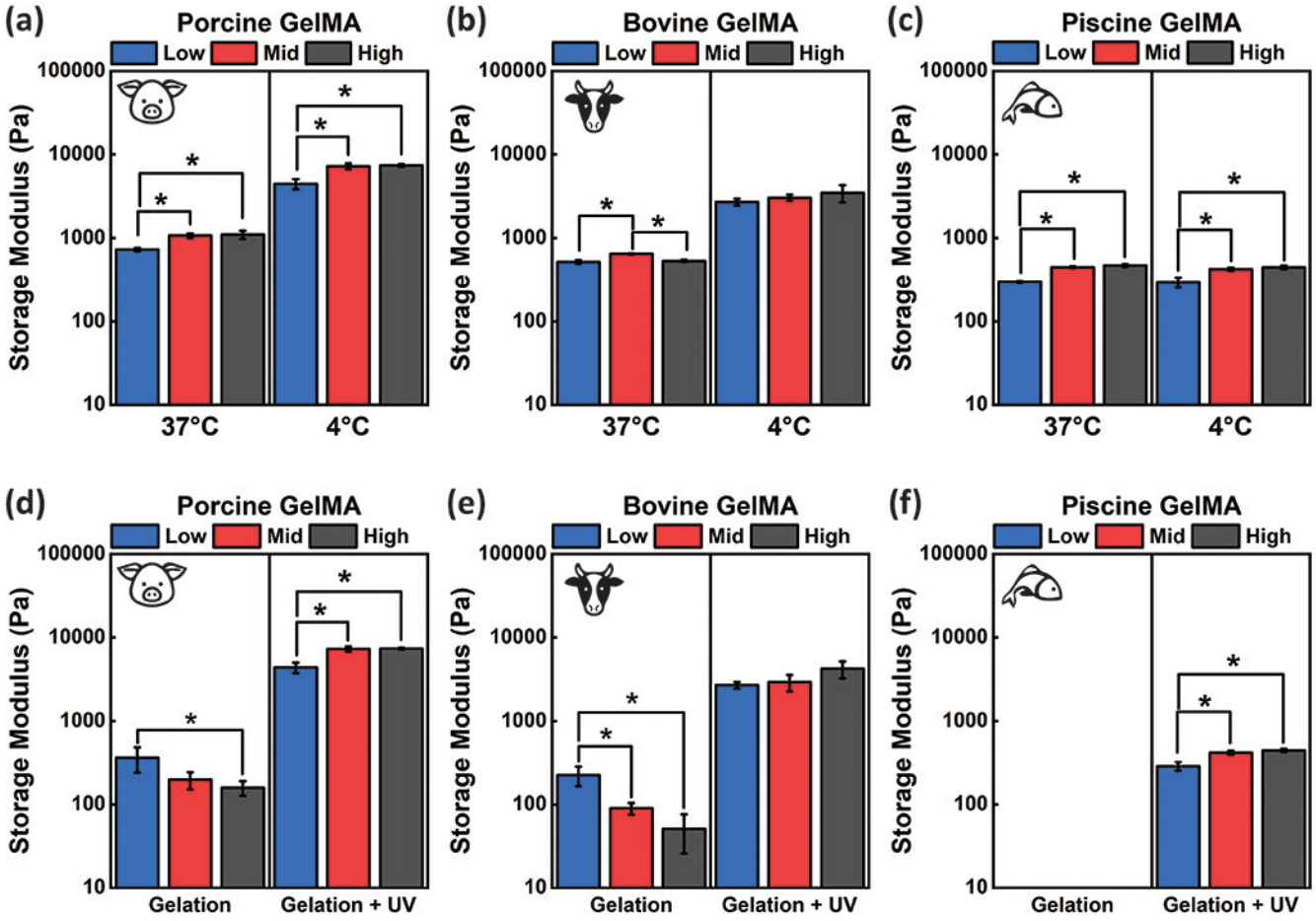

Figure 4.

Storage modulus (G') was compared for samples polymerized after incubation at 37 °C and 4°C for (a) porcine GelMA (b) bovine GelMA and (c) cold-water fish GelMA. Generally, storage modulus (G') increases with increasing DS. Porcine GelMA had higher storage moduli compared to samples synthesized from other sources and cold-water fish GelMA had the lowest. These measurements correlated to Bloom strength of unmodified gelatin. The trends noted for chemical crosslinking alone were conserved for dual crosslinked GelMA. Except for cold-water fish gelatin, which does not undergo physical gelation, GelMA samples demonstrated much higher storage moduli when dual crosslinked compared to chemical crosslinking alone. Storage modulus (G') measurements of physical crosslinks alone were compared to that of coordinated physical and chemical crosslinks for (d) porcine GelMA, (e) bovine GelMA, and (f) piscine GelMA. Statistical analysis included t-test comparisons with a p-value of 0.05 (n=9). Error bars are plotted as the standard deviation.

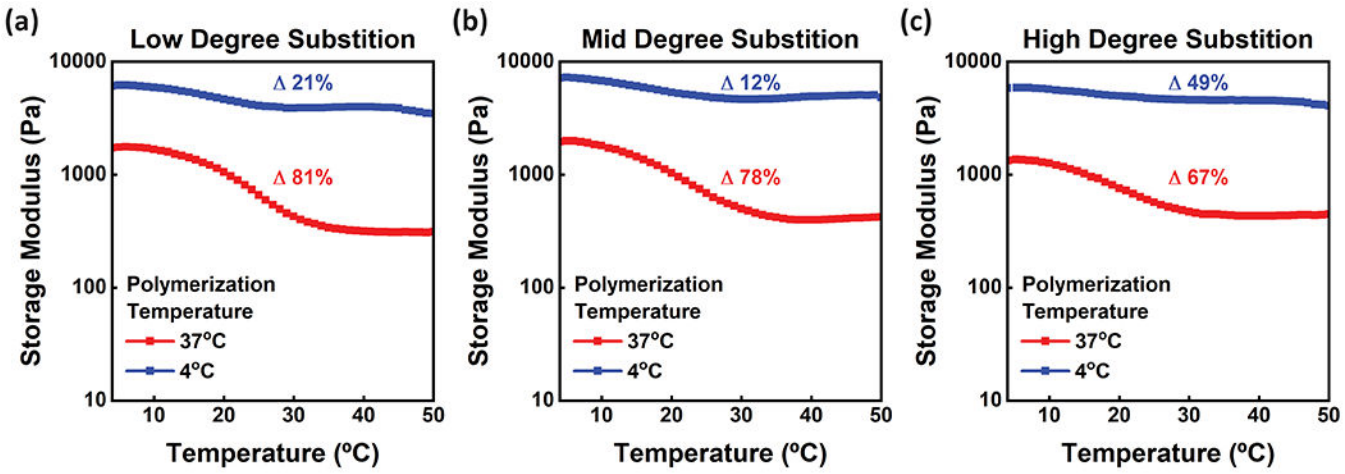

Figure 5.

Rheological measurements were collected sweeping from 4-50 °C for porcine samples at (a) low, (b) mid, and (c) high degrees of substitution. GelMA polymerized at 4 °C is shown in blue and GelMA polymerized at 37 °C is shown in red. GelMA with physical crosslinking alone and the lowest DS showed the highest change in storage modulus (G') between set temperatures, while the GelMA with the highest DS showed the lowest change in storage modulus (G'). GelMA crosslinked after incubation at 4°C showed less change in storage moduli with differing temperature compared to GelMA crosslinked at a warmer temperature. Data represents the average Storage modulus (G') across three replicates.

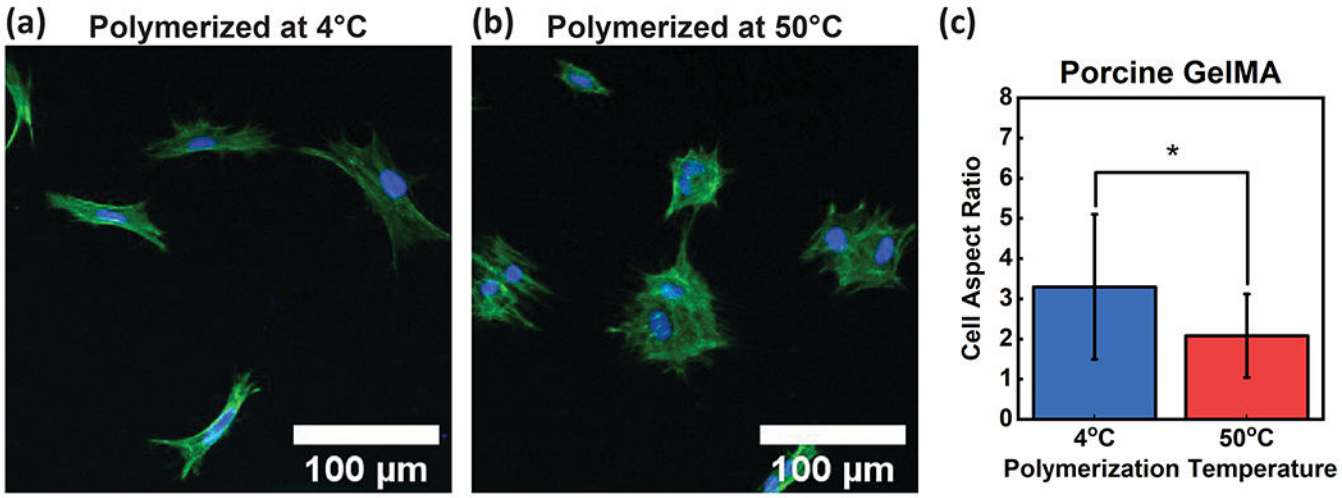

Figure 6.

Human dermal fibroblasts adopted different morphologies depending on matrix stiffness. (a) HDFns grown on porcine GelMA polymerized at 4°C showed a longer more fibril morphology, while (b) HDFns cultured on top of porcine GelMA polymerized at 50°C showed a rounder morphology and cytoskeletal organization. (c) HDFns grown on GelMA polymerized at 4°C had a significantly higher aspect ratio compared to those from softer porcine GelMA scaffolds polymerized at 50°C. Cells were analyzed at $n \geq 55$, imaged from 40X magnification. Statistical analysis included t-test comparisons with a p-value of 0.05. Error bars are plotted as the standard deviation.

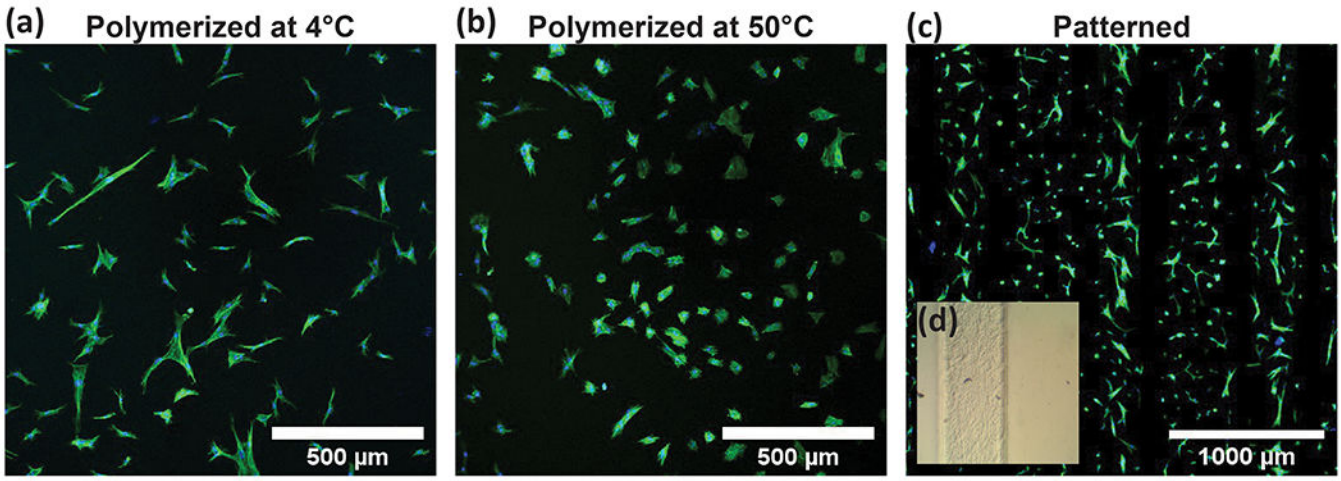

Figure 7.

(a) Longer and thinner HDFn morphologies on stiffer gels and (b) rounder HDFn morphologies on softer gels were observed in (c) porcine GelMA scaffolds patterned using lithography and temperature differences. (d) Brightfield images show clear lines between stiff GelMA polymerized at 4°C and soft GelMA polymerized at 50°C.

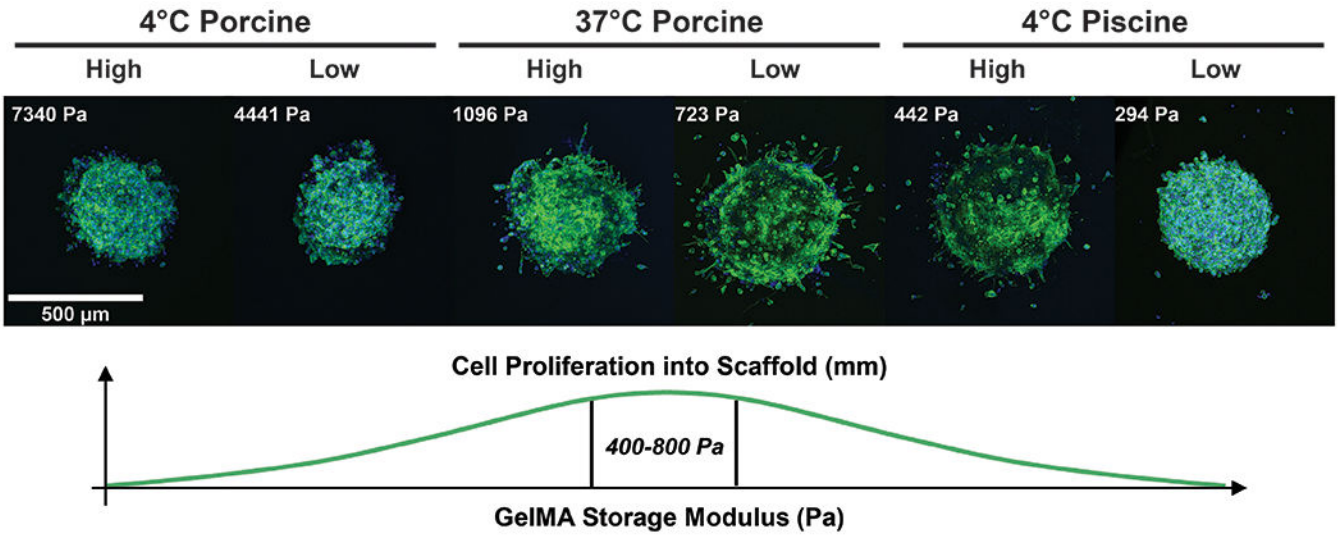

Figure 8.

MDAMB231 human mammary spheroids were cultured within GelMA scaffolds with different animal sources, degrees of substitution, and polymerization conditions. Phalloidin and DAPI stains were used to determine cell invasion into surrounding matrix. Stiffer matrices resulted in minimal spheroid outgrowth. Matrices with storage moduli between 400 and 1100 Pa demonstrated invasion into the surrounding matrix. The GelMA with the highest and lowest storage modulus (G') demonstrated minimal invasion into the surrounding matrix. Optimal cell proliferation was realized in hydrogels will storage moduli between 400 and 800 Pa.

Table 1.

Chemical properties and Bloom strength varied for each animal source depending on hydrolysis method and resultant GelMA type.

Source	Type	Hydrolysis Method	Bloom Strength	Molecular Weight	Isoelectric point
Porcine Skin *	A	Acid	300 g	50-100 kDa	7.0-9.0
Bovine Skin *	B	Lime	225 g	40-50 kDa	4.7-5.0
Cold-Water Fish Skin *	A	Acid	n/a	60 kDa	6

*Information provided by Millipore Sigma

Table 2.

Molecular weight between crosslinks was determined for each GelMA DS and polymerization temperature. The change in molecular weight between crosslinks between GelMA polymerized at 37°C and 4°C was determined for each gelatin source.

Source	Polymerization Temperature	Molecular Weight ($\overline{M_c}$) between Crosslinks (Da)			$\Delta\ \overline{M_c}$
		High DS	Mid DS	Low DS	
Piscine	**37°C**	16,394	22,846	24,548	2,439 (10%)
	4°C	23,013	23,285	24,805	
Bovine	**37°C**	16,021 to 19,077	15,370 to 18,162	16,060 to 19,134	8,092 (88%)
	4°C	8,433 to 9,210	8,597 to 9,406	9,332 to 10,292	
Porcine	**37°C**	15,383 to 22,219	15,289 to 22,024	17,060 to 25,896	13,563 (223%)
	4°C	4,909 to 5,444	4,978 to 5,529	7,208 to 8,422	